RSC Advances

ROYAL SOCIETY OF CHEMISTRY

www.rsc.org/advances

Synthesis of Ag_2CO_3/Bi_2WO_6 heterojunctions with enhanced photocatalytic activity and cycling stability

Jianxing Bao[a,b,c], Shenghui Guo[a,b,c], Jiyun Gao[d], Tu Hu[a,b,c], Li Yang[a,b,c*], Chenhui Liu[d], Jinhui Peng[a,b,c,d] and Caiyi Jiang[a,b,c]

a. State Key Laboratory of Complex Nonferrous Metal Resources Clean Utilization, Kunming University of Science and Technology, Kunming 650093, China

b.National Local Joint Laboratory of Engineering Application of Microwave Energy and Equipment Technology, Kunming 650093, China

c.Faculty of Metallurgical and Energy Engineering, Kunming University of Science and Technology, Kunming 650093, China

d.Key Laboratory of Comprehensive Utilization of Mineral Resources in National Regions, Yunnan Minzu University, Kunming 650031, China

Abstract

Hierarhical Bi_2WO_6 nanoarchitectures with scale of 2-3 μm were prepared *via* a facile microwave-assisted solution-phase reaction process. Monodispersed spherical Ag_2CO_3 nanoparticles with an average size of about 10 nm were deposited onto the surface of Bi_2WO_6 nanoarchitectures to form a novel Ag_2CO_3/Bi_2WO_6 heterojunction structure through a facile *in situ* precipitation-deposition method. The obtained samples were characterized by XRD, XPS, SEM, TEM (HRTEM), UV-vis DRS and nitrogen adsorption-desorption techniques. The photocatalytic evalution displays the decoration of Ag_2CO_3 nanoparticles significantly enhanced the photocatalytic activity of Bi_2WO_6 and the photocatalytic performance is greatly influenced by the content of deposited Ag_2CO_3. The 30 wt% Ag_2CO_3-loaded Bi_2WO_6 sample exhibited the highest photocatalytic activity for degradation of Rhodamine B (RhB) under visible light irradiation. Meanwhile, it possess also excellent cycling stability and superior photocatalytic performance toward other pollutants. The dramatic enhanced photocatalytic activity and stability can be mainly ascribed to well-matched energy band and heterojunction relative between Ag_2CO_3 and Bi_2WO_6, which can effective improve the separation of photo-induced electron-hole at the heterojunctional interfaces.

Keywords: Ag_2CO_3/Bi_2WO_6; Heterojunction structure; Visible light irradiation; Photocatalysis

1. Introduction

Heterogeneous photocatalysts have attracted tremendous attention due to their great potential for decomposing organic pollutants and for converting photon energy into chemical energy.[1-4] Among the novel photocatalysts, Bi_2WO_6 have been proven to be promising catalysts for photo-chemical reactions owing to theirs suitable bandgap (~2.8 eV) and strong oxidizing power.[5-7] The widely accepted that the photocatalytic performance of catalytic is very closely related to their surface structure and crystallinity including morphology, size, specific surface, crystal planes and defect.[8-10] Bi_2WO_6 as a layer-structured semiconductor, constructed by cornersharing WO_6 octahedra $(WO_4)^{2-}$ sheets and bismuth oxide $(Bi_2O_2)^{2+}$ sheets,[11] could be more easily obtained three-dimensional (3D) hierarchical architectures assembling by one-dimensional (1D) nanosheets. Many studies found that 3D hierarchical architectures could effectively increase the specific surface to volume ratio, organic pollutant adsorption and surface active sites.[12,13]

As is well known, excepting for adsorption behavior and photoresponse range of photocatalysts, as an ideal photocatalysts the separation efficiency and increase the oxidation power of photogenerated carriers is another vital consideration. Nonetheless, the bare Bi_2WO_6 photocatalysts has high recombination of photoinduced electron-hole (e^--h^+) pairs which leads to the low quantum efficiency.[14,15] Recent, numerous attempts have been made to prolong the lifetime of photogenerated e^--h^+ and promote carriers transport processes of Bi_2WO_6, including impurity doping,[16,17] noble metals sensitization,[18-20] and heterojunction structure formation.[21-28]

Coupling of two semiconducting structures with matching energy levels to form a heterojunction can effective improve absorb and utilizes to visible light. More importantly, the nanojunction system can remarkable changes the electrical properties of composite semiconductors, resulting in the enhanced separation, transport and oxidation (or reduction) power of photogenerated carriers.[29,30] Thus, coupling of

Bi_2WO_6 with other semiconductors have been widely employed to improve the photocatalytic performance of Bi_2WO_6. For *e.g.* $AgBr/Bi_2WO_6$, Ag_2S/Bi_2WO_6, $BiOBr/Bi_2WO_6$, TiO_2/Bi_2WO_6, Bi_2S_3/Bi_2WO_6 and $g\text{-}C_3N_4/Bi_2WO_6$ systems have been indicated as effectual in suppress the recombination of photogenerated e^--h^+ pairs.[21-28]

Recently, Ag_2CO_3 are regarded as a new high efficiency visible light photocatalysis material. Compared with the well-known N-doped TiO_2, the Ag_2CO_3 usually shows obviously excellent utilization rate of visible light and photocatalysis activity.[31,32] Although, Ag_2CO_3 is unstable in pure crystal form owing to its self-photocorrosion, previous studies suggested that Ag_2CO_3 could maintain its stability through growth heterostructured composites. Yu et al.[33] reported that the Ag_2O/Ag_2CO_3 heterostructured photocatalysts *via* phase transformation routes. This result indicates that the interface heterostructure effectively facilitates charge transfer and suppresses the recombination of photogenerated e^--h^+, resulting in exhibits extremely high activity and stability. Similarly, the synthesis of Ag_2CO_3 composite photocatalysts have been reported, such as $Ag_2CO_3/g\text{-}C_3N_4$, Ag_2CO_3/AgX, Ag_2CO_3/Ag/AgBr, and their visible-light-driven photocatalytic activity and stability have also been explored.[34-36] Herein, we intend to design a novel Ag_2CO_3/Bi_2WO_6 heterojunction photocatalyst with matching energy levels. This aim is to achieve improvement the visible-light photocatalytic activity of Bi_2WO_6 and overcome Ag_2CO_3 self-photocorrosion disadvantage.

Moreover, the microwave-assisted approach has been accepted as a promising method for the preparation of Bi_2WO_6.[37] Compared with traditional hydrothermal synthetic methods, microwave-assisted synthesis is simple, rapid, uniform, efficient, economical, and environmentally friendly.[38] Herein, in this work, we firstly prepared the Bi_2WO_6 microspheres using a facile microwave-assisted solution-phase reaction process. Then, monodispersed Ag_2CO_3 nanoparticles were deposited onto the surface of Bi_2WO_6 nanoarchitectures to form a novel Ag_2CO_3/Bi_2WO_6 heterojunction. As expected, as prepared the photocatalysts exhibited excellent photocatalytic activity and outstanding cycling performance for degradation the rhodamine B (RhB) dye

under visible light irradiation. Meanwhile, they also possess extremely high photocatalytic activities for other pollutants such as methyl orange (MO), methyl blue (MB), congo red (CR), and hexavalent chromium (Cr (VI)). Furthermore, the possible mechanism of enhanced photocatalytic activity and stability for Ag_2CO_3/Bi_2WO_6 heterojunctions was also discussed in detail.

2. Experiment section

2.1 Catalysts Synthesis

All the chemicals were analytic grade purity and used without further treatment. The hierarchical Bi_2WO_6 microspheres were prepared using a MARS 5 Microwave System (Matthews, NC, USA). In the system, the parameters of time and temperature of reaction are regulated by a user-defined computer program. The automatic temperature-control system allowed continuous monitoring and control of the internal temperature of the reaction system by continuously adjusting the applied microwave power. In a typical preparation procedure, $Bi(NO_3)_3•5H_2O$ (3.5 mmol) were dissolved in 5 mL acetic acid (36wt%) to form a clear solution by magnetic stirring, then 30 mL aqueous solution of $Na_2WO_4•2H_2O$ (2 mmol) was dropwise added to the obtained solution. The mixture was allowed to stir for another 1 h, then transferred to a 50 mL microwave (MW) teflon container and kept at 200 °C for 6 h.

For the synthesis of Ag_2CO_3/Bi_2WO_6 composites, the as-synthesized Bi_2WO_6 (0.5 mmol) powders were ultrasonic dispersed into 20 mL of deionized water. Subsequently, $AgNO_3$ solution (0.05 M) and $NH_3•H_2O$ solution (0.1 M) were added dropwise to the above suspension in sequence under magnetic stirring. At last, $NaHCO_3$ solution (0.05M) was added into the the mixture with a rate of less than 0.3 mL min^{-1}. The precipitate was collected by centrifugation, washed with deionized water and ethanol, and dried at 60 °C for 12 h. The Ag_2CO_3/Bi_2WO_6 composites with different mass ratios were fabricated by changing the added amount of $AgNO_3$, $NH_3•H_2O$ and $NaHCO_3$ solutions under the $AgNO_3/NH_3•H_2O/NaHCO_3$ volume ratios of 1:1:2. The samples are denoted as A-BWO-1, A-BWO-2, A-BWO-3 and A-BWO-4 when the weight percentages of Ag_2CO_3 in Ag_2CO_3/Bi_2WO_6 composites are 10%, 20%, 30%, 40%,

respectively. The pure Ag_2CO_3 were prepared by the same method without the addition of Bi_2WO_6. Moreover, the N-doped TiO_2 was obtained according to the literature reported.[39]

2.2 Characterization

The X-ray diffraction (XRD) datas were recorded on a Bruker D8 X-ray diffractometer with Cu-Kα radiation source (λ=1.5406 Å). Scanning electron microscopy (SEM) images were taken using a JSM-6701F scanning electron microscope with an accelerating voltage of 15 kV. Energy Dispersive X-ray (EDX) analysis was also performed on the JSM-6701F. Transmission electron microscopy (TEM) images were obtained on a JEM-2100 electron microscope at an accelerating voltage of 200 kV. The X-ray photoelectron spectroscopy (XPS) analysis was recorded though an AXIS-ULTRA DLD-600W photoelectron spectrometer with Al K1 radiation. The UV-vis diffuse reflectance spectroscopy (DRS) obtained using Hitachi U-4100 spectrophotometer. Nitrogen adsorption-desorption isotherms were collected on an Autosorb-iQ sorption analyzer and analyzed followed by the Brunauer-Emmett-Teller (BET) equation and Barret-Joyner-Halenda (BJH) model.

2.3 Photocatalytic activity test

The photocatalytic performance of the as-prepared samples was evaluated by measuring the degradation of RhB. In a typical photocatalytic measurement, the samples (0.1 g) were put into a solution of RhB dyes (100 mL, 10 mg/L), which was then irradiated with a 300W Xe arc lamp to provide visible light with $\lambda \geq 420$ nm by an cutoff filter. Before the suspensions were irradiated they were magnetically stirred for 60 min in the dark to complete the adsorption-desorption equilibrium between dyes and photocatalysts. The degradation results were analyzed by using the UV-vis spectrophotometer (UV-2550, Shimadzu, Japan). Before the spectroscopy measurement, these photocatalysts were removed from the photocatalytic reaction systems by centrifugation. The same test for the RhB was also carried out on MB, MO and CR. The Cr (VI) was tested using the diphenylcarbazide (DPC) method introduced by Clesceri et al.[40]

3. Results and discussion

3.1 Structure and property analysis

The structural characteristics and phase composition of samples were investigated by powder XRD. As shown in Fig. 1, the diffraction peaks of pure Bi_2WO_6 and Ag_2CO_3 samples can be match well with the standard crystalline structure of the orthorhombic phase of Bi_2WO_6 (JCPDS no. 73-1126) and the monoclinic phase of Ag_2CO_3 (JCPDS no. 70-2184), respectively. For Ag_2CO_3/Bi_2WO_6 heterojunctions samples, excepting for all the diffraction peaks of Bi_2WO_6, the peaks at 2θ of 18.6°, 20.5°, 32.6°, 33.6°, 37.1°, 39.6°, 44.3°, and 51.3° are attributed to the pure monoclinic phase of Ag_2CO_3. Meanwhile, the intensities of corresponding diffraction peaks of Ag_2CO_3 strengthened gradually along with the increase of the Ag_2CO_3 content in Ag_2CO_3/Bi_2WO_6 composites. Metallic Ag or impurity peaks was not detected from any of the samples, indicating that Ag_2CO_3/Bi_2WO_6 composites are only composed of Ag_2CO_3 and Bi_2WO_6 phases.

The elemental composition and oxidation states of the as-prepared samples were further analyzed by XPS. Fig. 2a shows XPS survey spectra of pure Bi_2WO_6, Ag_2CO_3 and A-BWO-3 composite. The overview spectrum of composite demonstrates that Bi, W, O, C and Ag exist, further confirming that the sample was composed of Bi_2WO_6 and Ag_2CO_3. Fig. 2b-f show the high-resolution spectra of Bi 4f,W 4f, O 1s, C 1s and Ag 3d regions for the A-BWO-3 sample, respectively. The peaks at binding energies (E_b) of 163.3 and 158.0 eV (Fig. 2b) belong to Bi $4f_{5/2}$ and Bi $4f_{7/2}$ of Bi^{3+} ions,[41] which shift toward low binding energy compared with that of pure Bi_2WO_6 (164.7 and 159.4 eV, Fig. S2). The appearance was also found in the XPS spectra of W 4f and O 1s. Such results could be ascribed to the interaction between Bi_2WO_6 and Ag_2CO_3 resulting in an inner shift of Bi 4f, W 4f and O 1s orbits.[42] The W $4f_{5/2}$ and W $4f_{7/2}$ peaks (Fig. 2c) located at 36.3 and 34.2 eV with a spin-orbit separation of 2.1 eV, which corresponds to W^{6+} according to previous reports.[43] The wide and asymmetric XPS of O 1s peaks (Fig. 2d) can be deconvoluted into four peaks, the peaks at E_b of 528.9, 529.7 and 530.5 eV correspond to Bi-O, W-O and crystal lattice oxygen of

Ag_2CO_3, respectively.[44,45] The weak peak at 531.7 eV correspond to surface absorbed oxygen species.[46] In Fig. 2e, the C 1s spectrum were deconvoluted into three peaks: the peaks at E_b of 283.6 eV could be attributed to carbon element in Ag_2CO_3, which is similar to what was reported by Dong et al,[47] and the rest of two peaks were mainly ascribed to the adventitious hydrocarbon from XPS itself. Fig. 2f gives the high-resolution XPS spectrum of Ag 3d. The peaks at E_b of 366.9 and 372.9 eV correspond to the Ag $3d_{5/2}$ and Ag $3d_{3/2}$ of Ag^+, respectively.[22] It is clear suggesting that no metal Ag is formed, which is in accordance with the result of XRD analysis. Therefore, by combining XPS and XRD investigation, the results confirmed that there were both Bi_2WO_6 and Ag_2CO_3 species in the Ag_2CO_3/Bi_2WO_6 composite samples.

The morphology of the as-synthesized samples was examined by SEM, as shown in Fig. 3. It can be clearly seen that the bare Bi_2WO_6 is uniformly dispersed and presents 3D hierarchical architectures with a diameter of 2-3 μm (Fig. 3a). When Ag_2CO_3 was deposited onto 3D hierarchical Bi_2WO_6 microspheres via a facile precipitation-deposition process (Fig. 3b-e), the resulting Ag_2CO_3/Bi_2WO_6 composite exhibits a similar morphology and size as compared to that of bare Bi_2WO_6. With increasing Ag_2CO_3 content, it is easy to observe that the large amount Ag_2CO_3 nanoparticles were dispersed uniformly onto the surface of hierarchical Bi_2WO_6 microspheres. Furthermore, the EDX spectrum of A-BWO-3 composite is shown in Fig. 3f. The composite is only contain Bi, W, O, C and Ag elements except for the elements of Au from the supports, which is well consistent with the XRD and XPS results.

Further information regarding the microstructure of prepared samples was obtained from TEM and HRTEM images. Fig. 4a and b show TEM images of the bare Bi_2WO_6 with different magnifications. It is easy to observe that the hierarchical Bi_2WO_6 microspheres with a zigzag brim, which is in fact assembled by several laminar Bi_2WO_6 nanoplates with quadrate shape. Specifically, each quadrate shape nanoplate has a relative smooth surface with an average length of about 60 nm and a width of

about 40 nm. Fig. 4c and d show TEM images of the A-BWO-3 composite. The locations of Ag_2CO_3 nanoparticles on the surface of Bi_2WO_6 nanoplates are indicated by arrows in TEM (Fig. 4d). It displays that some monodispersed spherical nanoparticles with size of about 10 nm covered the surface of Bi_2WO_6 nanoplates. Fig. 4e is the corresponding selected area electron diffraction (SAED) pattern of composite, which shows several diffraction rings, indicating that the nanoplates are polycrystalline structure . The diffraction fringes can be indexed to (113), (006), (206) and (313) planes for the orthorhombic crystal structure of Bi_2WO_6, which is in accordance with XRD results. HRTEM (Fig. 4f) shows that Ag_2CO_3 nanoparticles tightly adhere to the surfaces of Bi_2WO_6 nanoplates. The lattice fringe spacings of 0.315 and 0.266 nm correspond to the (113) plane of orthorhombic Bi_2WO_6 and the (130) plane of monoclinic Ag_2CO_3, respectively. Thus, the above results indicate the formation of heterojunctions between Ag_2CO_3 and Bi_2WO_6.

Fig. 5 shows the fabrication method of the Ag_2CO_3/Bi_2WO_6 heterojunction photocatalysts via a three-step process. Firstly, Bi_2WO_6 hierarchical microspheres obtained by a facile microwave-assisted solution-phase reaction process. Afterwards, the $AgNO_3$ solution and $NH_3•H_2O$ were added to the Bi_2WO_6 suspension. The formation of $Ag(NH_2)^{2+}$ can be bound tightly to the surface of hierarchical Bi_2WO_6 microspheres due to chemical adsorption. After that, with the addition $NaHCO_3$, $Ag(NH_2)^{2+}$ ions attached to the surface of Bi_2WO_6 react with HCO_3^- to generate Ag_2CO_3 nanoparticles. Furthermore, added $NH_3•H_2O$ is an important influencing factor for the regulation of Ag_2CO_3 grain size and formation of nano-heterojunctions. In the absence of $NH_3•H_2O$, a large number of short nanorods of Ag_2CO_3 are existing on the brim of Bi_2WO_6 nanoplates (Fig. S3).

Fig. 6 displays the nitrogen adsorption-desorption isotherms and the corresponding pore size distribution curves of the as-prepared Bi_2WO_6 and A-BWO-3 heterojunction photocatalysts. The isotherm of samples can be categorized as a type IV isotherm and an H3-type hysteresis loop ($0.75<P/P_0<0.99$), suggesting the presence of mesoporous structures with silt-like pores in these two samples.[48]

According to the fitting analysis with the BET equation, the surface area of hierarchical Bi_2WO_6 microspheres is about 19.2 m^2g^{-1}. After decoration with Ag_2CO_3 nanoparticles, the heterojunction photocatalysts still possesses a relatively large surface area of 16.8 m^2g^{-1}. Furthermore, the main pore size distribution (inset of Fig. 6) in these two samples is similarly in the range of 10-15 nm, thus implying the Ag_2CO_3 nanoparticles only covered the surface of Bi_2WO_6 and the pore size was retained well.

The light absorption properties of the as-prepared samples were investigated by UV-visible diffuse reflectance spectra. As shown in Fig. 7, the absorption spectrum of pure Bi_2WO_6 extends from UV region to visible light at about 450 nm. Compared with pure Bi_2WO_6, the Ag_2CO_3/Bi_2WO_6 heterojunctions shows a significant redshift of absorption edge and displays surprisingly strong absorption around 450-800 nm. This observation clearly indicates that the Ag_2CO_3/Bi_2WO_6 heterojunctions show more intensive absorption within the visible light range. This could be extremely advantageous for the degradation of pollutants owing to the light harvest ability great impact to the photocatalytic reaction process. Furthermore, it could be seen that the improvement of visible light absorption intensity is unconspicuous with increasing Ag_2CO_3 content. It might be because the excess Ag_2CO_3 will impede the light contacting with Bi_2WO_6 crystal and inhibit interfacial transport of electron-hole between Ag_2CO_3 and Bi_2WO_6.[49] In addition, the optical band gaps was calculated following the equation: [50]

$$\alpha h\nu = \mathrm{A}(h\nu - E_g)^{n/2}$$

where α, h, ν, A and E_g are absorption coefficient, planks constant, frequency, proportionality constant and bandgap, respectively. And n value is determined by the type of transition (n value is 4 for Ag_2CO_3 and Bi_2WO_6 with indirect transition).[19,33,51] A plot of $(\alpha h\nu)^{1/2}$ *versus* $(h\nu)$ gives the bandgap as shown in the insets of Fig. 7. The bandgap of Ag_2CO_3 and Bi_2WO_6 estimated from the intercept of the tangent to the plot are 2.17 and 2.74 eV, respectively. The bandgap of as-prepared pure Ag_2CO_3 is lower than that of Ag_2CO_3 crystals (~2.30 eV) obtained by reaction

of $NaHCO_3$ with $AgNO_3$.[33,34] It could be attributed to the different the preparation method and phase composition of Ag_2CO_3.

3.2 Photocatalytic activity

The photocatalytic performance of as-prepared samples was evaluated by the degradation of RhB and MO under visible light irradiation. For comparison, the respective performance of P25 and prepared N-doped TiO_2 (N-TiO_2) photocatalysts was also presented and the results are given in Fig. 8. As shown in Fig. 8 a, the RhB can only be slightly degraded under visible light irradiation without catalysts, indicating that the self-degradation effect of RhB could be ignored. Compared to pure Ag_2CO_3 and Bi_2WO_6, the Ag_2CO_3/Bi_2WO_6 heterojunctions can effectively improve the photocatalytic activities. The highest activity is observed in A-BWO-3 sample, and the degradation rate to RhB can exceed 95% within 60 min. Additionally, it is noted that the A-BWO-3 heterojunction photocatalysts exhibit remarkably superior photocatalytic activity under the same conditions compared to P25 and N-TiO_2. Fig. 8b shows the absorption spectral changes of RhB solution with the temporal evolution. The major absorption peaks of RhB around 553 nm diminished gradually with the increasing visible light irradiation time in the presence of the A-BWO-3. Meanwhile, the suspension losses of color gradually, which further indicates that the structure of RhB have been destroyed. The pseudo-first-order reaction kinetic of the photocatalytic for the degradation of RhB solution was investigated and the results are given in Fig. S4 and Table 1. The rate constant k is 0.0489 min^{-1} for A-BWO-3 heterojunction photocatalysts, which is much higher than those of P25 (0.0014 min^{-1}), N-TiO_2 (0.0124 min^{-1}), pure Ag_2CO_3 (0.0195min^{-1}) and pure Bi_2WO_6 (0.0272min^{-1}). This results indicated RhB could be degraded more efficiently by A-BWO-3 heterojunction photocatalysts.

Furthermore, MO was also selected as the other typical target compound to further evaluate the photocatalytic activity of as-prepared samples. As shown in Figure 8c and d, the A-BWO-3 is decomposed about 95.2% of MO after 50 min under visible light irradiation. For comparison, only 4.7%, 13.2%, 43.1%, and 54.8% of MO is

removed under the same conditions for pure Bi_2WO_6, P25, N-TiO_2 and pure Ag_2CO_3, respectively. The photodegradation process of MO was found to follow pseudo-first-order kinetics and the rate constant over the A-BWO-3 heterojunction photocatalysts is higher than the sum of pure Bi_2WO_6 and pure Ag_2CO_3 (Fig. S4 and Table 1). The photocatalytic decomposition rate constant of A-BWO-3 over MO is 35 and 5 times over P25 and N-TiO_2. Moreover, the data, showed in Table 1, revealed the heterojunction photocatalysts for decomposition of RhB is more related to Ag_2CO_3 content. It is ascribed that the synergistic effect between Bi_2WO_6 and Ag_2CO_3 play a dominant role in reaction process. Whereas, for degradation of MO, the significantly enhanced the photocatalytic activity of Bi_2WO_6 is mainly due to the modification effect of Ag_2CO_3 to Bi_2WO_6. It can thus be seen that the actual active component of heterojunction photocatalysts for the degradation of RhB and MO is different. At the same time, the experimental data showed that the photocatalytic activity of Ag_2CO_3/Bi_2WO_6 enhanced remarkably with increasing Ag_2CO_3 content. Nevertheless, Ag_2CO_3 content exceeds 30 wt%, the photocatalytic activity decreased, suggesting that the optimal Ag_2CO_3 content in Ag_2CO_3/Bi_2WO_6 is 30 wt%. The optimum content of Ag_2CO_3 in heterojunction should be related to the recombination rate of photogenerated e^--h^+ pairs and light absorption efficiency. The similar phenomenon was also observed other systems such as Ag_2CO_3/g-C_3N_4,[34] AgBr/Ag_2CO_3.[52]

To further investigate the validity of photocatalytic activity of A-BWO-3 heterojunction photocatalysts, the degradation experiments of A-BWO-3 for other pollutants such as MB, CR, and Cr (VI) were performed. As shown in Fig. 9, the A-BWO-3 heterojunction photocatalysts could remove more than 95% of these pollutants after 60 min. All these results convincingly demonstrate that the formation of heterogenous interface in Ag_2CO_3/Bi_2WO_6 can effectively promote the photoactivity of pure Bi_2WO_6.

3.3 Catalyst stability

The stability of catalysts is a vital consideration except for the photocatalytic activity in practical applications. Thus, the stability of the pure Ag_2CO_3 and A-BWO-3 was investigated. As shown in Fig. 10, it was found that the Ag_2CO_3 nanoparticles almost lose their activity in after two recycles. This results can due to the reduction of large amounts Ag^+ ions in Ag_2CO_3 lattice by the photogenerated electrons ($Ag_2CO_3 + 2e^- \rightarrow 2Ag^0 + CO_3^{2-}$) during the recycles reaction.[31,32] The excessive Ag could act as the recombination center of electrons and prevent the visible light absorption of Ag_2CO_3, leading to the photocatalytic activity extremely lower. Conversely, the A-BWO-3 still maintains 85% degradation rate after five recycles for RhB. Fig. S5 and S6 show the XRD and XPS of the freshly obtained A-BWO-3 and its recovered samples after cycles of photocatalysis. It is found that there is a slight change in position and intensity of peaks after five cycles of photodegradation reaction, demonstrating that the Ag_2CO_3 remain stable and only a relatively small number of of Ag^0 nanoparticles were formed on the surface of Ag_2CO_3.

3.4 Possible photocatalytic mechanism

To confirm the main active species in the photocatalytic process, we performed *in situ* trapping experiments of free radicals and holes for degradation of RhB by A-BWO-3 heterojunction system. As shown in Fig. 11, disodium ethylenediaminetetraacetate (EDTA, a quencher of h^+), 1,4-benzoquinone (BQ, a quencher of $\bullet O^{2-}$) and isopropanol (IPA, a •OH scavenger) was added into the reaction liquid. We observed that the addition of 2 mM EDTA had a significant effect on the k_{app} compared with no scavenger under same conditions, suggesting that h^+ may play a dominant role in the photocatalytic reaction process of RhB degradation. Whereas, after the addition of 2 mM IPA or BQ had a relatively lesser influence on the k_{app}, meaning that •OH and $\bullet O^{2-}$ played a secondary role and to a lesser extent participated in the photocatalytic reaction process.

For the hierarchical Ag_2CO_3/Bi_2WO_6 heterojunctions, the enhancement mechanism of photocatalytic activity could be further revealed by the energy band matching principle for two semiconductors. The top of the valence band (VB) and the bottom

of the conduction band (CB) of Ag_2CO_3 were calculated to be 2.60 and 0.43 eV (*vs*. NHE), respectively. And the VB and CB of Bi_2WO_6 were estimated to be 3.23 and 0.49 eV (*vs*. NHE), (some relevant details of the energy band estimation were provided in the *Supporting Information*). It was widely accepted that the excellent photocatalytic activity results from an efficient separation and smooth transport of photogenerated electrons and holes, a schematic illustration of the possible heterojunction enhancement mechansim for photocatalytic activity in Ag_2CO_3/Bi_2WO_6 was shown in Fig. 12. It can be seen the electron is excited from the valence band to the conduction band in both Ag_2CO_3 and Bi_2WO_6 , thereby generating an electron-hole pairs under visible light irradiation. Once the formation of heterogeneous interfaces between Bi_2WO_6 and Ag_2CO_3, the photogenerated electrons on the Ag_2CO_3 nanoparticles will easily transfer to the CB of Bi_2WO_6 through the closely contacted interfaces in that Ag_2CO_3 has a more negative potential of the conduction band and valence band than that of Bi_2WO_6. Meanwhile the photoinduced holes could migrate from the VB of Bi_2WO_6 to that of Ag_2CO_3. Therefore, the photoexcited electrons and holes are separated effectively due to the ingenious heterojunction design under visible light irradiation. Meanwhile, the photocorrosion of Ag_2CO_3 nanoparticles can be further restrained because photoinduced electrons will fast transfer to the CB of Bi_2WO_6 rather than react with the Ag^+ ions of Ag_2CO_3 ($Ag^+ + e^- \rightarrow Ag^0$). The captured electrons on the CB of Bi_2WO_6 can be react with dissolved oxygen to give $\bullet O^{2-}$.[53] And the holes with strong oxidizing power in the VB of Ag_2CO_3 can be react with H_2O to generate •OH or directly oxidize pollutants adsorbed.[36,54] Based on the above results, we believe that the well-matched band of the Ag_2CO_3/Bi_2WO_6 heterojunctions can promote interfacial carriers transfer processes and prolong the lifetime of photogenerated holes and electrons , resulting in high photocatalytic activity and stability.

In addition, after cycle of photodegradation reaction, a small number of Ag were formed on the surface of Ag_2CO_3 (Fig. S5 and S6), which can act as an electron-rich collective.[32] These enriched electrons on Ag^0 nanoparticles will participate in the

multi-electron transfer routes ($O_2 + 2e^- + 2H^+ = H_2O_2$ (aq.); $O_2 + 4e^- + 4H^+ = 2H_2O$ (aq.)).[55] While Ag^0 may also become a recombination center of e^--h^+ pairs,[56] but also overmuch Ag^0 nanoparticles on the Ag_2CO_3 surface could prevent the visible ligh absorption of Ag_2CO_3,[34] which would lead to the decrease of activity in recycling reactions. With increasing cyclic tests, a relatively stable Ag-Ag_2CO_3 system can be formed. The self-stability mechanism has also been discussed in some other silver-contained compounds.[57,58] Therefore, Ag-Ag_2CO_3/Bi_2WO_6 system may be a vital factor for high stability in the photocatalytic reaction process.

4. Conclusion

In summary, a novel hierarchical Ag_2CO_3/Bi_2WO_6 heterojunctions catalyst has been successfully fabricated by *in situ* depositing monodispersed spherical Ag_2CO_3 nanoparticles onto the surface of Bi_2WO_6. The decoration of Ag_2CO_3 nanoparticles significantly enhanced the photocatalytic activity of Bi_2WO_6 and the 30 wt% Ag_2CO_3 content sample exhibited the highest photocatalytic activity for degradation of RhB and MO. Furthermore, Ag_2CO_3/Bi_2WO_6 heterojunctions have excellent cycling stability. The enhanced photocatalytic activity and stability is not only attributes to the narrow bandgap of Ag_2CO_3 and extended the optical response, but also benefits by the appropriate band structure matching to enhanced the photo-generated carriers separation in the heterogenous interface between Ag_2CO_3 and Bi_2WO_6. Consequently, we believe that such heterojunction system is promising extended to other silver-containing heterostructured photocatalysts with highly efficient photocatalytic performances.

Acknowledgements

This work was supported by the National Natural Science Foundation of China (No. 51264015), Yunnan Provincial Science and Technology Innovation Talents scheme -Technological Leading Talent of China (No. 2013HA002), The Applied Basic Research Fund Project of Yunnan Province & Kunming University of Science and Technology of China (No. 14118930), as well as the Kunming Scientific and

Technological Project of China (No. 2014-04-A-H-02-3085).

References

[1] A. Kudo and Y. Miseki, Chem. Soc. Rev., 2009, 38, 253-278.

[2] S. Y. Dong, J. L. Feng, M. H. Fan, Y. Q. Pi, L. M. Hu, X. Han, M. L. Liu, J. Y. Sun and J. H. Sun, Rsc Adv., 2015, 5, 14610–14630.

[3] M. Anpo and M. Takeuchi, J. Catal., 2003, 216, 505–516.

[4] J. Tian, Y. H. Sang, G. W. Yu, H. D. Jiang, X. N. Mu and H. Liu, Adv. Mater., 2013, 25, 5075-5080.

[5] A. Kudo and S. Hijii, Chem. Lett., 1999, 1103-1104.

[6] L. W. Zhang, Y. J. Wang, H. Y. Cheng, W. Q. Yao and Y. F. Zhu, Adv. Mater., 2009, 21, 1286-1290.

[7] H. F. Cheng, B. B. Huang, Y. Y. Liu, Z. Y. Wang, X. Y. Qin, X. Y. Zhang and Y. Dai, Chem. Commun., 2012, 48, 9729-9731.

[8] H. L. Xu, W. Z. Wang, W. Zhu, J.Phys. Chem.B, 2006, 110, 13829-13834.

[9] H. Wang, J. Gao, T. Q. Guo, L. Guo and J. H. Li, Chem. Commun., 2011, 48, 275-277.

[10] D. S. Kim, S. Y. Kwak, Appl. Catal. A-Gen., 2007, 323, 110-118.

[11] F. Amano, K. Nogami and B. Ohtani, J. Phys. Chem. C, 2009, 113, 1536-1542.

[12] Z. Chen, L. W. Qian, J. Zhu, Y. P. Yuan and X. F. Qian, CrystEngComm, 2010, 12, 2100-2106.

[13] F. Cao, W. D. Shi, L. J. Zhao, S. Y. Song, J. H. Yang, Y. Q. Lei and H. J. Zhang, J. Phys. Chem. C, 2008, 112, 17095-17101.

[14] J. Ren, W. Z. Wang, S. M. Sun, L. Zhang and J. Chang, Appl. Catal. B-Environ., 2009, 92, 50-55.

[15] C. M. Liu, J. W. Liu, G. Y. Zhang, J. B. Zhang, Q. S. Wu, Y. Y. Xu and Y. Q. Sun, Rsc Adv., 2015, 5, 32333-32342.

[16] M. Shang, W. Z. Wang, L. Zhang and H. L. Xu, Mater. Chem. Phys., 2010, 120, 155-159.

[17] S. Guo, X. F. Li, H. Q. Wang, F. Dong and Z. B. Wu, J. Colloid Interf. Sci., 2012, 369(5):373–380.

[18] T. L. Thompson and J. T. Yates, Chem. Rev., 2006, 106, 4428-4453.

[19] D. J. Wang, G. G. Xue, Y. Z. Zhen, F. Fu and D. S. Li, J. Mater. Chem, 2012, 22, 4751-4758.

[20] J. Yang, X. H. Wang, Y. M. Chen, J. Dai and S. H. Sun, Rsc Adv., 2015, 5, 9771-9782.

[21] D. J. Wang, L. Guo, Y. Z. Zhen, L. L. Yue, G. G. Xue and F. Fu, J. Mater. Chem. A, 2014, 2, 11716-11727.

[22] O. Mehraj, B. M. Pirzada, N. A. Mir, S. Suitana and S. Sabir, Rsc Adv., 2015, 5, 42910-42912.

[23] Y. L. Li, Y. M. Liu, J. S. Wang, E. Uchaker, Q. F. Zhang, S. B. Sun, Y. N. Huang, J. Y. Li and G. Z. Cao, J. Mater. Chem. A, 2013, 27, 7949-7956.

[24] Y. F. Hou, S. J. Liu, J. H. Zhang, X. Cheng and Y. Wang, Dalton Trans, 2014, 43, 1025-1031.

[25] M. Shang, W. Z. Wang, L. Zhang, S. M. Sun, L. Wang and L. Zhou, J. Phys. Chem. C, 2009, 113, 14727-14731.

[26] Z. J. Zhang, W. Z. Wang, L. Wang and S. M. Sun, Acs Appl. Mater. Inter., 2012, 4, 593-597.

[27] Y. J. Wang, X. J. Bai, C. G. Pan, J. He and Y. F. Zhu, J. Mater. Chem, 2012, 22,11568-11573.

[28] Y. L. Tian, B. B. Chang, J. L. Lu, J. Fu, F. N. Xi and X. P. Dong, Acs Appl. Mater. Inter., 2013, 5, 7079-7085.

[29] X. F. Gao, W. T. Sun, G. Ai and L. M. Peng, Appl. Phys. Lett., 2010, 96, 153104-3.

[30] H. F. Cheng, B. B. Huang, P. Wang, Z. Y. Wang, Z. Z. Lou, J. P. Wang, X. Y. Qin, X. Y. Zhang and Y. Dai, Chem. Commun., 2011, 47, 7054-7056.

[31] S. H. Guo, J. X Bao, T. Hu, L. B. Zhang, L. Yang, J. H. Peng and C. Y. Jiang, Nanoscale Res. Lett., 2015, 10, 1-8.

[32] G. P. Dai, J. G. Yu and G. Liu, J. Phys. Chem. C, 2012, 116, 15519-15524.

[33] C. L. Yu, G. Li, S. Kumar, K. Yang and R. C. Jin, Adv. Mater., 2014, 26, 892-898.

[34] Y. F. Li, L. Fang, R. X. Jin, Y. Yang, X. Fang, Y. Xing and S. Y. Song, Nanoscale, 2015, 7, 758-764.

[35] H. J. Dong, G. Chen, J. X. Sun, Y. J. Feng, C. M. Li, G. H. Xiong and C. D. Lv, Dalton Trans., 2014, 43, 7282-7289.

[36] J. J. Li, Y. L. Xie, Y. J. Zhong and Y. Hu, J. Mater. Chem. A, 2015, 3, 5474-5481.

[37] X. F. Cao, L. Zhang, X. T. Chen and Z. L. Xue, CrystEngComm, 2010, 13, 306-311.

[38] L. K. Pan, X. J. Liu, Z. Sun and C. Q. Sun, J. Mater. Chem. A, 2013, 1, 8299-8326.

[39] B. Chi, L. Zhao and T. Jin, J. Phys. Chem. C, 2007, 111, 6189-6193.

[40] L. S. Clesceri, A. E. Greenberg and A. D. Eaton, American Public Health Association, Washington, 1998, pp. 366-368.

[41] J. Wu, F. Duan, Y. Zheng and Y. Xie, J. Phys. Chem. C, 2007,111, 12866-12871.

[42] T. Yan, Q. Yan, X. D. Wang, H. Y. Liu, M. M. Li, S. X. Lu, W. G. Xu and M. Sun, Dalton Trans., 2015, 44, 1601-1611.

[43] H. P. Li, W. G. Hou, X. T. Tao and N. Du, Appl. Catal. B-Environ., 2015, 172-173, 27-36.

[44] W. J. Yang, B. Ma, W. C. Wang, Y.W. Wen, D. W. Zeng and B. Shan, Phys. Chem. Chem. Phys., 2013, 15, 19387-19394.

[45] C. Dong, K. L. Wu, X. W. Wei, X. Z. Li, L. Liu, T. H. Ding, J. Wang and Y. Ye, CrystEngComm, 2014, 16, 730-736.

[46] D. J Wang, Y. Z. Zhen, G. L. Xue, F. Fu, X. M. Liu and D. S. Li, J. Mater. Chem. C, 2013, 1, 4153-4162.

[47] H. J. Dong, G. Chen, J. X. Sun, C. M. Li, Y. G. Yu and D. H. Chen, Appl. Catal. B-Environ., 2013, 134-135, 46-54.

[48] T. S. Natarajan, H. C. Bajaj and R. J. Tayade, CrystEngComm, 2014, 17, 1037-1049.

[49] J. X. Xia, J. Di, S. Yin, H. Xu, J. Zhang, Y. G. Xu, L. Xu, H. M. Li and M. X. Ji, Rsc Adv., 2014, 4, 82–90.

[50] M. A. Butler, J. Appl. Phys., 1977, 48, 1914–1920.

[51] C. M. Li, G. Chen, J. X. Sun, Y. J. Feng, J. J. Liu and H. J. Dong, Appl. Catal. B-Environ., 2015, 163, 415-423.

[52] H. Xu, J. X. Zhu, Y. X. Song, W. K. Zhao, Y. G. Xu, Y. H. Song, H. Y. Ji and H. M. Li, RSC Adv., 2014, 4, 9139-9147.

[53] W, J. Yang, B. Ma, W. C. Wang, Y. W. Wen, D. W. Zeng and B. Shan, Phys. Chem. Chem. Phys., 2013, 15, 19387-19394.

[54] L. S. Zhang, K. H. Wong, H. Y. Yip, H. Chun, J. C. Yu, C. Y. Chan and P. K. Wong, Environ. Sci. Technol., 2010, 44, 1392-1398.

[55] H. G. Yu, R. Liu, X. F. Wang, P. Wang and J. G. Yu, Appl. Catal. B-Environ., 2012, 111-112, 326-333.

[56] R. Georgekutty, M. K. Seery and S. C. Pillai, J. Phys. Chem. C, 2008, 112, 13563-13570.

[57] H. G. Yu, L. Liu, X. F. Wang, P. Wang, J. G. Yu and Y. H. Wang, Dalton Trans., 2012, 41, 10405-10411.

[58] X. F. Wang, S. F. Li, H. G. Yu, J. G. Yu and S. W. Liu, Chem. - Eur. J., 2011, 17, 7777-7780.

Table

Table 1. Pseudo-first-order rate constants in photocatalytic degradation RhB (k_1) and MO (k_2).

Sample	k_1 (min^{-1})	k_2 (min^{-1})
Pure-Ag_2CO_3	0.0195	0.0132
Pure-Bi_2WO_6	0.0272	0.0005
A-BWO-1	0.0297	0.0110
A-BWO-2	0.0343	0.0342
A-BWO-3	0.0489	0.0598
A-BWO-4	0.0423	0.0532
Degussa P25	0.0014	0.0017
prepared N-TiO_2	0.0124	0.0108

Figure

Fig. 1 XRD patterns of the pure Bi_2WO_6 , Ag_2CO_3 and Ag_2CO_3/Bi_2WO_6 composite photocatalyst with different Ag_2CO_3 content.

Fig. 2 XPS survey spectra (a) and high-resolution XPS spectra of Bi 4f (b),W 4f (c) O 1s (d), C 1s (e) and Ag 3d (f) regions for A-BWO-3 composite.

Fig. 3 SEM images of bare Bi_2WO_6 (a), A-BWO-1 (b), A-BWO-2 (c), A-BWO-3 (c) and A-BWO-4 (d) composite photocatalysts; EDX spectrum of A-BWO-3 composite photocatalysts (f).

Fig. 4 TEM images of bare Bi_2WO_6 (a , b) and A-BWO-3 heterojunction photocatalysts (c , d); SAED and HRTEM of A-BWO-3 heterojunction photocatalysts (e, f).

Fig. 5 Schematic diagram of the fabrication of Ag_2CO_3/Bi_2WO_6 heterojunctions.

Fig. 6 Nitrogen adsorption-desorption isotherms and the corresponding pore size distribution curves (inset) of the pure Bi_2WO_6 and the A-BWO-3 heterojunction photocatalysts.

Fig. 7 UV-vis diffuse reflectance spectra of the as-prepared samples and the bandgap (inset) of the pure Bi_2WO_6 and pure Ag_2CO_3.

Fig. 8 Photocatalytic activity of as-prepared samples and the adsorption spectra in the presence of A-BWO-3 for degradation of RhB (a, b) and MO (c, d) under visible irradiation.

Fig. 9 Photocatalytic activity of A-BWO-3 for degradation of MB, CR, Cr (VI), MO and RhB after 60 min visible light irradiation.

Fig. 10 The recycling tests of the as-prepared Ag_2CO_3 and A-BWO-3 heterojunction photocatalysts for photodegradation of RhB.

Fig. 11 Comparison of the rate constant k_{app} of photocatalytic degradation RhB by A-BWO-3 in the presence of various scavengers, the concentration of all added scavengers is 2 mM.

Fig. 12 Schematic illustration photocatalytic reaction process and the possible charge carriers transfer of the Ag_2CO_3/Bi_2WO_6 heterojunctions under visible light irradiation.

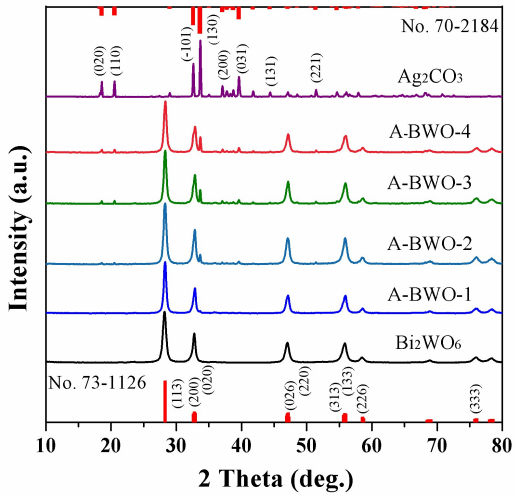

Fig. 1 XRD patterns of the pure Bi_2WO_6, Ag_2CO_3 and Ag_2CO_3/Bi_2WO_6 composite photocatalyst with different Ag_2CO_3 content.

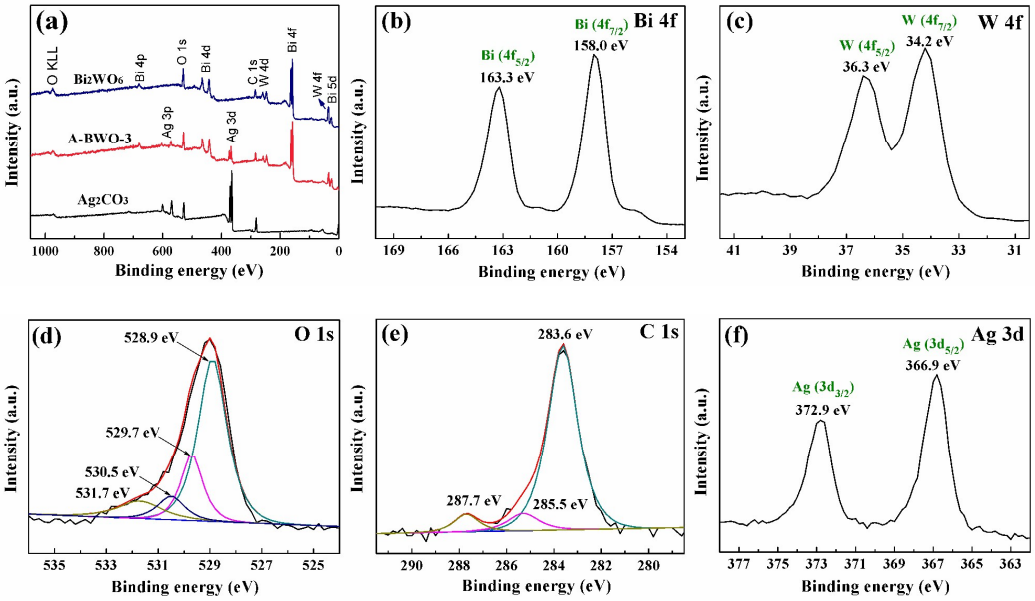

Fig. 2 XPS survey spectra (a) and high-resolution XPS spectra of Bi 4f (b),W 4f (c) O 1s (d), C 1s (e) and Ag 3d (f) regions for A-BWO-3 composite.

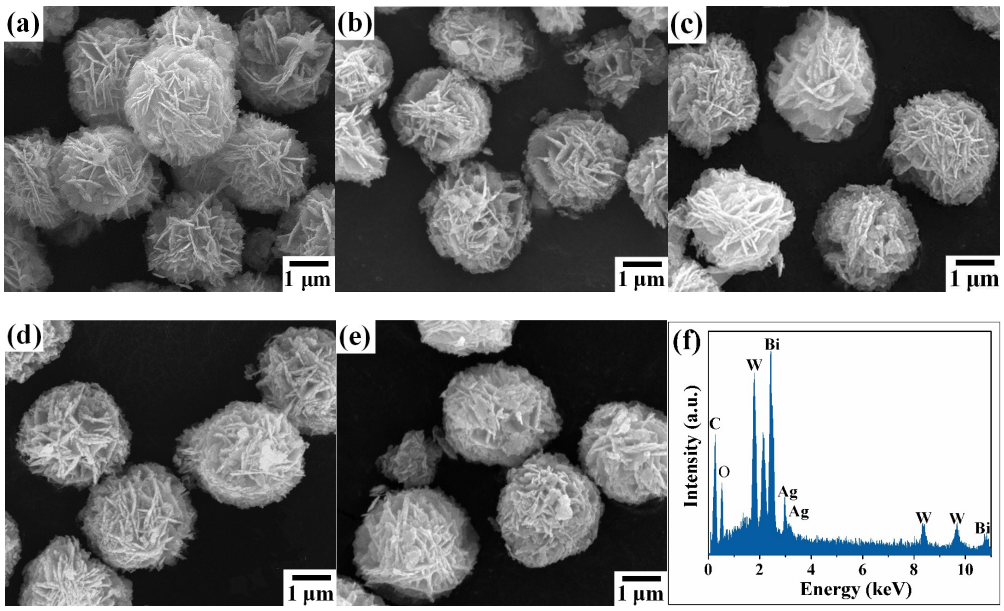

Fig. 3 SEM images of bare Bi_2WO_6 (a), A-BWO-1 (b), A-BWO-2 (c), A-BWO-3 (c) and A-BWO-4 (d) composite photocatalysts; EDX spectrum of A-BWO-3 composite photocatalysts (f).

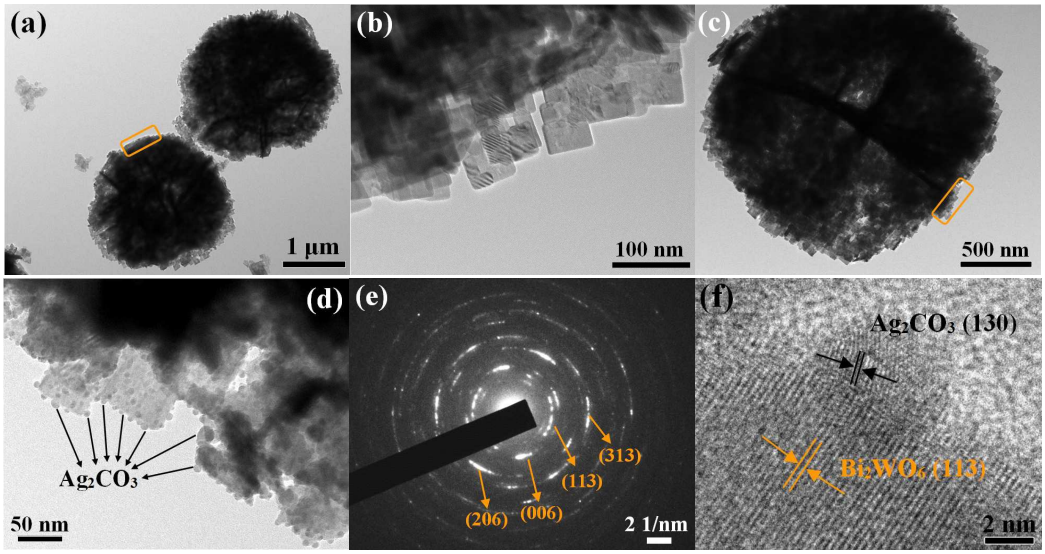

Fig. 4 TEM images of bare Bi_2WO_6 (a , b) and A-BWO-3 heterojunction photocatalysts (c , d); SAED and HRTEM of A-BWO-3 heterojunction photocatalysts (e, f).

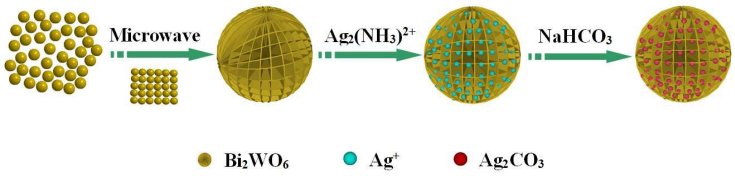

Fig. 5 Schematic diagram of the fabrication of Ag_2CO_3/Bi_2WO_6 heterojunctions.

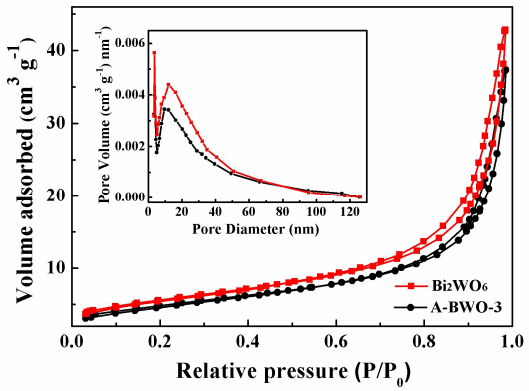

Fig. 6 Nitrogen adsorption-desorption isotherms and the corresponding pore size distribution curves (inset) of the pure Bi_2WO_6 and the A-BWO-3 heterojunction photocatalysts.

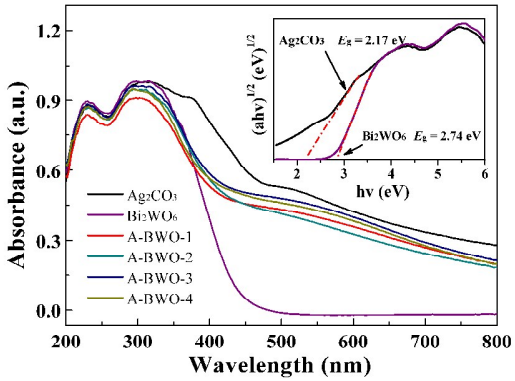

Fig. 7 UV-vis diffuse reflectance spectra of the as-prepared samples and the bandgap (inset) of the pure Bi_2WO_6 and pure Ag_2CO_3.

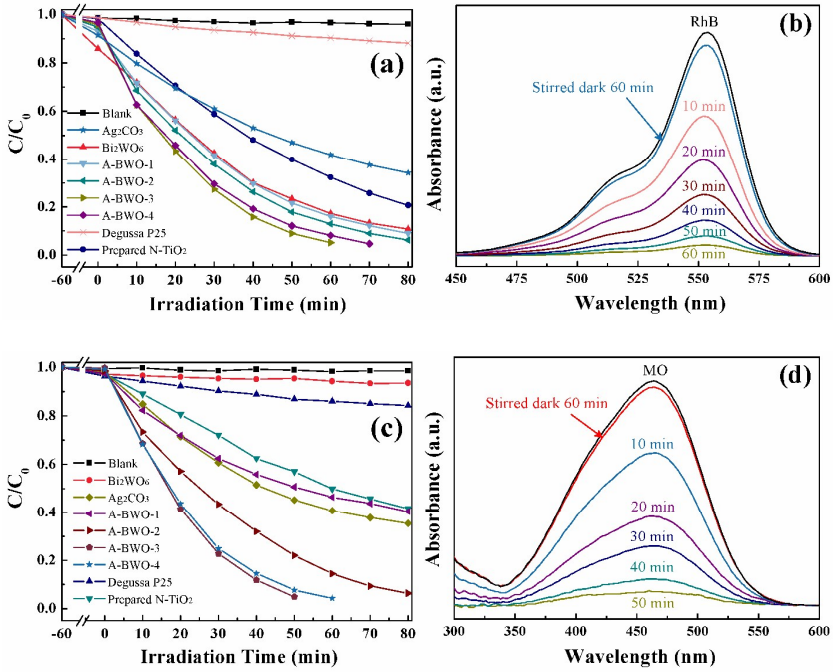

Fig. 8 Photocatalytic activity of as-prepared samples and the adsorption spectra in the presence of A-BWO-3 for degradation of RhB (a, b) and MO (c, d) under visible irradiation.

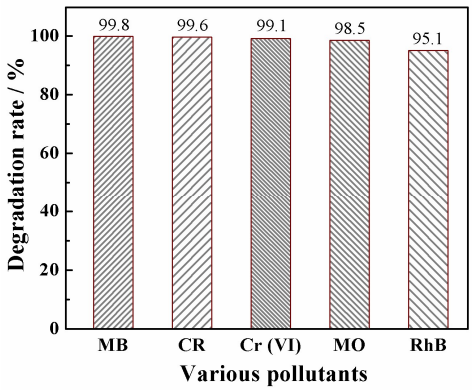

Fig. 9 Photocatalytic activity of A-BWO-3 for degradation of MB, CR, Cr (VI), MO and RhB after 60 min visible light irradiation.

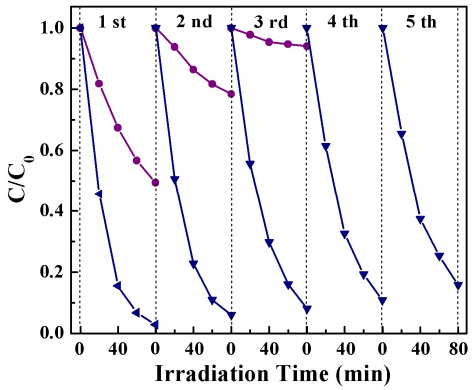

Fig. 10 The recycling tests of the as-prepared Ag_2CO_3 and A-BWO-3 heterojunction photocatalysts for photodegradation of RhB.

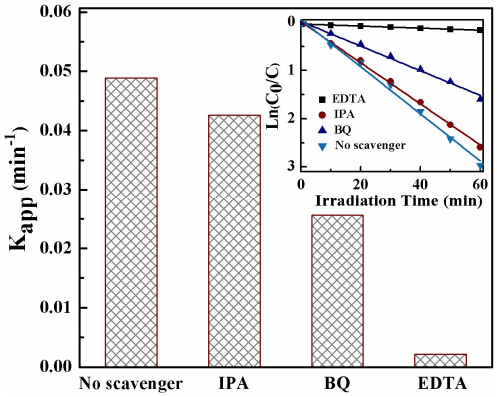

Fig. 11 Comparison of the rate constant k_{app} of photocatalytic degradation RhB by A-BWO-3 in the presence of various scavengers, the concentration of all added scavengers is 2 mM.

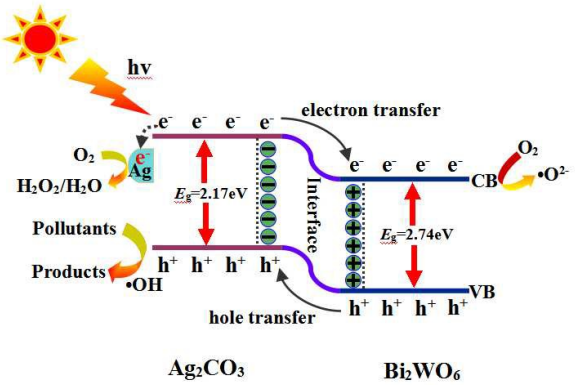

Fig. 12 Schematic illustration photocatalytic reaction process and the possible charge carriers transfer of the Ag_2CO_3/Bi_2WO_6 heterojunctions under visible light irradiation.